Catalysis Today 144 (2009) 7–12

Contents lists available at ScienceDirect

Catalysis Today

journal homepage: www.elsevier.com/locate/cattod

Synthesis, characterization and electronic structure of nitrogen-doped TiO_2 nanopowder

Katarzyna Anna Michalow [a,b,*], Dmitry Logvinovich [c], Anke Weidenkaff [c], Martin Amberg [d], Giuseppino Fortunato [d], Andre Heel [b,**], Thomas Graule [b], Mieczyslaw Rekas [a]

[a] Faculty of Material Science and Ceramics, AGH University of Science and Technology, al. Mickiewicza 30, 30-059 Krakow, Poland
[b] Laboratory for High Performance Ceramics, EMPA Swiss Federal Laboratories for Materials Testing and Research, Ueberlandstrasse 129, 8600 Duebendorf, Switzerland
[c] Solid State Chemistry and Catalysis, EMPA Swiss Federal Laboratories for Materials Testing and Research, Ueberlandstrasse 129, 8600 Duebendorf, Switzerland
[d] Laboratory for Advanced Fibers, EMPA Swiss Federal Laboratories for Materials Testing and Research, Lerchenfeldstrasse 5, 9014 St. Gallen, Switzerland

ARTICLE INFO

Article history:
Available online 25 January 2009

Keywords:
N-doped TiO_2
Nanopowders
Photocatalysts
Electronic structure
Optical properties

ABSTRACT

Nanopowders of TiO_2:N were synthesized in a two step process. At first, TiO_2 was prepared from titanium tetraisopropoxide (TTIP) in form of crystalline powder by flame spray synthesis (FSS). In a second step TiO_2-FSS with a specific surface area (SSA) of 54 m^2/g and TiO_2-P25 as a reference material were ammonolysed in a rotating tube furnace. X-ray diffraction (XRD) and transmission electron microscopy (TEM) were used to investigate crystallinity before and after ammonolysis. Based on the X-ray photoelectron spectroscopy (XPS) studies it has been established that the N 1s peak at 395.9 eV can be assigned to substitutional nitrogen. New electron transitions and resulting band gap changes in respect to undoped sample have been observed in $TiO_{2-x}N_x$. Diffusive reflectance and the resulted band gap energy were determined by diffuse reflection spectroscopy (DRS), where the correlation between differential reflectance and Tauc plot, known as a second method of the band gap determination, is discussed for pure and N-doped TiO_2 nanopowders. The photocatalytic performance of the nanopowders under visible light irradiation (400–500 nm) was studied by the degradation of methylene blue (MB) in aqueous suspensions.

1. Introduction

Recently, the anion-doped TiO_2 has attracted considerable attention due to its reported photocatalytic activity in the visible light [1–6]. Among all so-called second-generation photocatalysts, the N-doped TiO_2 seems to be the most promising. However, the explanation of the role of the nitrogen is controversially discussed. Asahi et al. [1] described photoactivity of TiO_2:N in the range below 500 nm by methylene blue (MB) and acetaldehyde gas decomposition, whereas Mrowetz et al. [4] argued that N-TiO_2 is unable to decompose MB through a photooxidation reaction under visible irradiation. Another controversial issue is the mechanism of nitrogen incorporation into the TiO_2 lattice (substitutional or interstitial) [5] as well as the effect of N-incorporation on the electronic structure of the TiO_2 [6]. The optical properties and resulting band gap position, determined by spectroscopic measurements showed a noticeable shift of light absorption towards to the visible region [1–6].

Many ways of preparation of the TiO_2:N have been reported so far. An often used preparation is heat treatment of TiO_2 under NH_3 atmosphere. Different types of TiO_2 have been used as a starting material such as amorphous [3], anatase or rutile single crystals [2], as well as a mixture of both polymorphic TiO_2 forms known as TiO_2-P25 (Degussa) [5]. However the reported results draw the conclusion, that anatase with a high specific surface area is the most suitable TiO_2 for ammonolysis.

The present study reports on the TiO_2-FSS and TiO_2-P25 nanopowders investigated for their potential use in preparation of N-doped nanostructured TiO_2 photocatalysts with a focus on structural, optical properties and photocatalytic activity under visible light. The methods of estimation of the optical properties through the application of the Tauc plot and differential reflectance for the band gap calculation are discussed in detail.

2. Experimental

2.1. Synthesis of TiO_2 and $TiO_{2-x}N_x$ nanoparticles

2.1.1. Flame spray synthesis (FSS)

Nanopowders of TiO_2 with defined specific surface area (SSA) were produced by a flame spray synthesis (FSS) using titanium tetraisopropoxide (TTIP; $Ti(C_3H_7O)_4$, purity > 99%, VWR) dissolved in

* Corresponding author at: AGH University of Science and Technology, Faculty of Material Science and Ceramics, al. Mickiewicza 30, 30-059 Krakow, Poland. Tel.: +48 504 794099.
** Corresponding author.
E-mail addresses: katarzynamichalow@o2.pl (K.A. Michalow), andre.heel@empa.ch (A. Heel).

0920-5861/$ – see front matter © 2008 Elsevier B.V. All rights reserved.
doi:10.1016/j.cattod.2008.12.015

ethanol (EtOH; 99%, Sigma–Aldrich) as a precursor. Details of the synthesis and the setup of the FSS plant are reported elsewhere [7,8]. The total flow rate of the precursor solution was 0.13 $cm^3\ s^{-1}$. The precursor was dispersed by a constant flow of oxygen (583 $cm^3\ s^{-1}$) by a gas-assisted external mixing nozzle. The resulting aerosol was ignited by acetylene-oxygen flamelets (C_2H_2: 217 $cm^3\ s^{-1}$; O_2: 283 $cm^3\ s^{-1}$). Product particles were collected in a bag-house filter and representative samples of about 1–2 g were collected on glass fibre filters (GF/A 150, Whatman) via a bypass and using vacuum pumps.

2.1.2. Ammonolysis

The reaction of the oxides with ammonia gas (PanGas, 99.98%, 2.5 $cm^3\ s^{-1}$) was carried out at T = 550 °C (heating rate: 10 K/min) in a rotating cavity quartz (SiO_2) reactor [9] with an internal diameter of 30 mm. The mass of both samples TiO_2-FSS (F-TiO_2) and TiO_2-P25 (P-TiO_2) was 0.25 g. During the reaction time of 4 h, the ammonia was supplied through a quartz tube with a diameter of 5.8 mm placed above the sample. After the reaction the samples were quenched down to room temperature within 2 min under ammonia flow. The obtained samples, referred to as F-$TiO_{2-x}N_x$ (TiO_2-FSS as starting material) and P-$TiO_{2-x}N_x$ (TiO_2-P25 as starting material) were annealed at T = 350 °C for 10 min in ambient air.

2.2. Characterization of the photocatalysts

The primary particle size, shape and morphology of the particles were investigated by transmission electron microscopy (TEM; Philips CM30) operating at 300 kV.

Structure, phase composition and size-strain parameters of the starting and reacted powders were studied by X-ray powder diffraction (XRPD) using a Philips X'Pert PRO MPD Θ–Θ System (Cu Kα radiation) equipped with a linear detector X'Celerator. Crystallographic and microstructural parameters were obtained from Rietveld refinement of the XRPD data, recorded using in the 2Θ angular range of 22–123° with a step size of 0.017° and a counting time of 200 s/step. The background was modelled by 6-coefficient polynomial function. The reflection shape was modelled with a Thompson-Cox-Hastings pseudo-Voigt profile function [10] corrected for asymmetry [11,12]. Applying that function allows extracting the samples intrinsic profile by using the known instrumental profile and performing a line broadening analysis to conclude about particle size and strain [13]. The instrumental profile was obtained from the measurement of LaB_6 SRM 660a standard. All the refinements were performed using Fullprof [14]. The observed isotropic line broadening was accounted for by refining isotropic size-strain components (in Fullprof referred to as Y and U) of the sample intrinsic profile.

The band gap energy E_g was determined with a Lambda 19 PerkinElmer double beam spectrophotometer. It is equipped with a 200 mm integrating sphere, used to measure the spectral dependence of total and diffuse reflectance over a wavelength λ of 250–2500 nm. Powder samples were measured in 1 mm thick quartz cell (Quartz Suprasil, Hellma). The reflectance of Spectralon (LabSphere) was used as a reference (R_{ref}).

XPS measurements were performed in order to study chemical composition and the oxidation states of the surface elements in TiO_2:N nanopowders, using a PHI LS 5600 instrument equipped with a standard Mg KαX-ray source. The energy resolution of the spectrometer was set at 0.8 eV/step at a pass energy of 187.85 eV for survey scans and 0.25 eV/step at 58.70 eV pass energy for region scans. The X-ray beam was operated at a current of 25 mA and an acceleration voltage of 13 kV. Charge effects were corrected using Carbon 1s = 287.85 eV. The elemental concentrations of the surface species were determined using CasaXP software (peak areas using the instrument specific relative sensitivity factors).

2.3. Photocatalytic experiments

Details of the photochemical reactor are reported elsewhere [8,15]. In brief, the photochemical irradiation system comprised two half-cylinders, each of which contained six Hg T5 lamps (400–500 nm, λ_{max} = 435 nm) for the visible light irradiation. The reaction vessel was a double-walled 125 cm^3 quartz Drechsel bottle with a rubber septum through which the samples where extracted. Thermostated water (30 °C) was pumped continuously through the outer jacket of the reaction vessel. The pollutant liquid consists of an aqueous solution of 5.15×10^{-5} M methylene blue (deionized water, pH 5.5). The powder concentration in the solution was adjusted at 0.4 mg/cm^3. Degradation experiments were carried out at pH 5.5 for MB. The reaction dispersion was continuously purged with air (110 cm^3/min) and magnetically stirred (300 rpm) throughout the irradiation period. Extracted samples were filtered through 0.2 μm nylon membrane filters to remove the photocatalyst particles before analysis by a Cary 50 UV–Vis spectrophotometer. Calibration of the absorbance at 664 nm against MB concentration was carried out for the determination of the photocatalytic activity and concentration was determined from the peak intensity.

3. Results and discussion

White nanopowder of TiO_2-FSS was obtained by flame spray synthesis (FSS) referred to as F-TiO_2 and had a specific surface area 54 $m^2\ g^{-1}$, comparable to TiO_2-P25 from Degussa referred to as P-TiO_2. Ammonolysed powders had a greenish colour, which can be due to the presence of Ti^{3+} (blue tint). After annealing under ambient air the colour of the F-$TiO_{2-x}N_x$ (TiO_2-FSS doped with N) and P-$TiO_{2-x}N_x$ (TiO_2-P25 doped with N) powders turn to bright orange colour. The yellow or orange colour of the ammonolysed powders was already reported and was assigned to $TiO_{2-x}N_x$ material [1,16].

Spherical, non-aggregated particles were observed by TEM before (Fig. 1a) and after (Fig. 1b) ammonolysis. Fig. 1c shows that during ammonolysis some particles rupture along the grain boundaries, what was confirmed by the decrease of the average crystallite size after ammonolysis (Table 1).

The crystalline phases of the pure and N doped TiO_2 nanopowders were analyzed by X–ray diffraction. The diffraction pattern of all investigated powders can be seen in Fig. 2 and the results of the refinement are listed in Table 1. Anatase was the predominant phase in all cases: a decrease of 3.12% for F-$TiO_{2-x}N_x$ and 0.45% for P-$TiO_{2-x}N_x$ of the anatase phase was observed in the samples after ammonolysis. N-doped samples do not exhibit additional phases except anatase and rutile. For P-TiO_2 the average crystallite size of the rutile was bigger and the anatase average crystallite size was smaller, than for F-TiO_2. The crystallinity increased where the average crystallite size of both phases of the ammonolysed powders decreased, what can be seen in the diffraction pattern as weaker and broader peaks, while exceptional average crystallite size of anatase of P-$TiO_{2-x}N_x$ is slightly smaller than the one of starting material. The decrease in the crystallite size can be related to the rupture of the polycrystals under influence of ammonium atmosphere pressure as shown in Fig. 1c.

Anatase lattice parameter a is slightly increased after ammonolysis and anatase lattice parameter c is slightly decreased, resulting in an increase of the cell volume (Table 1). The observed changes in the cell parameters can be related to the incorporation of N into the TiO_2 lattice, while additional defects due to the anion-type of doping oxygen vacancies are introduced [17].

The XPS analyses of the F-TiO_2 before and after ammonolysis were carried out in order to determine the chemical composition of the valence states of the atoms. The binding energies obtained

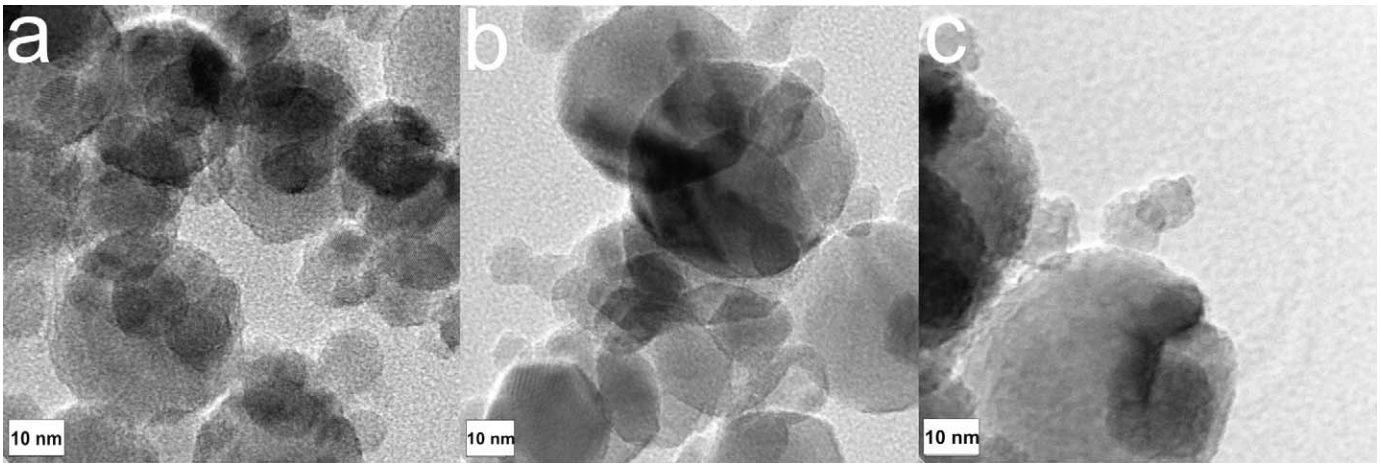

Fig. 1. TEM image of F-TiO_2 (a) and (b) and F-$TiO_{2-x}N_x$ nanopowder (c).

Table 1
Summary of data obtained by X-ray diffraction measurements of pure and N-doped TiO_2 nanopowders (Fig. 2).

Sample	F-TiO_2		F-$TiO_{2-x}N_x$		P-TiO_2		P-$TiO_{2-x}N_x$	
	Anatase	Rutile	Anatase	Rutile	Anatase	Rutile	Anatase	Rutile
Fraction (wt.%)	91.07 ± 0.45	8.93 ± 0.20	88.23 ± 0.56	11.77 ± 0.26	83.13 ± 0.39	16.87 ± 0.14	82.75 ± 0.47	17.25 ± 0.17
Average crystallite size (nm)	27.72	11.85	20.96	10.87	20.58	34.99	21.06	32.41
Lattice parameter, *a* (nm)	0.3786 ± 0.0001	0.4592 ± 0.0001	0.3787 ± 0.0001	0.4591 ± 0.0001	0.3786 ± 0.0001	0.4594 ± 0.0001	0.3787 ± 0.0001	0.4595 ± 0.0001
Lattice parameter, *c* (nm)	0.9505 ± 0.0001	0.2956 ± 0.0001	0.9503 ± 0.0001	0.2958 ± 0.0001	0.9508 ± 0.0001	0.29588 ± 0.0001	0.9507 ± 0.0001	0.2960 ± 0.0001
Cell volume (nm^3)	0.1362 ± 0.0001	0.0623 ± 0.0001	0.1363 ± 0.0001	0.0623 ± 0.0001	0.1362 ± 0.0001	0.0624 ± 0.0001	0.1363 ± 0.0001	0.0625 ± 0.0001

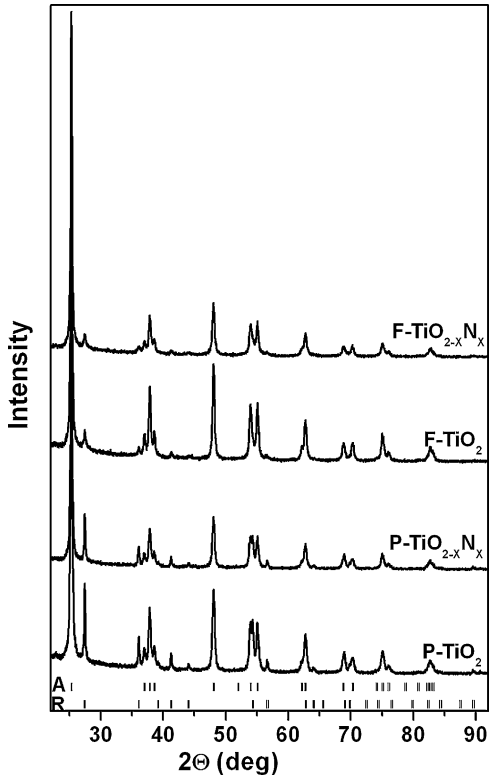

Fig. 2. XRD pattern of the P-TiO_2, P-$TiO_{2-x}N_x$, F-TiO_2 and F-$TiO_{2-x}N_x$. Symbols A and R indicate anatase and rutile phases, respectively.

from the curves fitted to Ti $2p_{3/2}$ data were at 458.6 and 458.5 eV for F-TiO_2 and F-$TiO_{2-x}N_x$, respectively. These values are in agreement with already reported 458.7 eV for the Ti in the 4+ oxidation state [18]. The O 1s peak was narrow with a shoulder in the direction of the higher binding energy for both nanopowders, pure and N-doped F-TiO_2. The O 1s peak at 529.8 eV was fitted by two curves: the dominant O $1s_I$ peak was attributed to TiO_2 and the minor O $1s_{II}$ was attributed to hydroxyl groups or water adsorbed

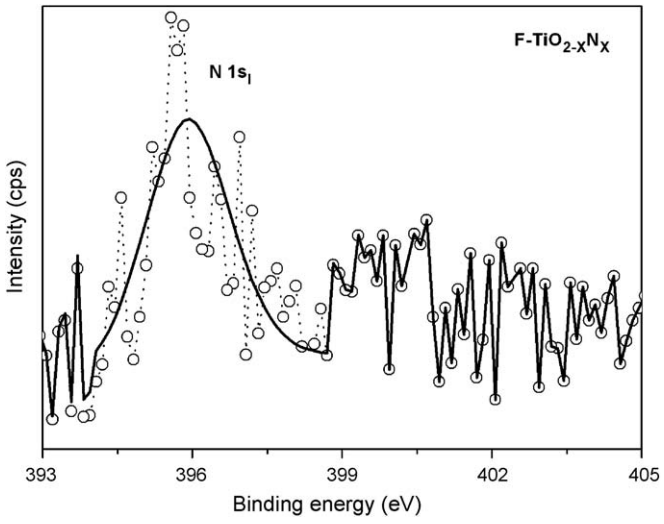

Fig. 3. N 1s XPS spectra of F-$TiO_{2-x}N_x$ nanopowder.

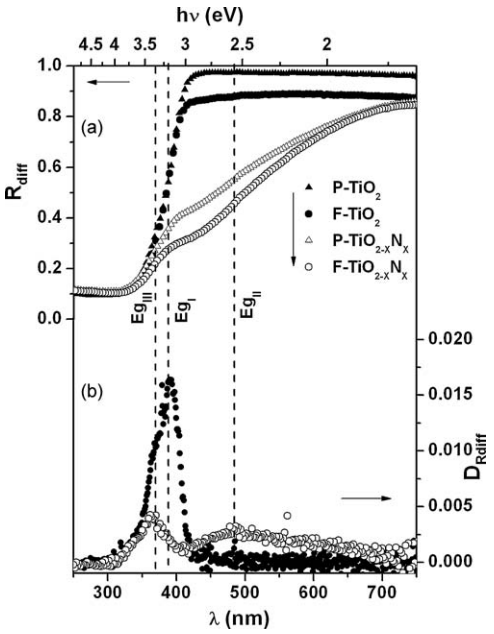

Fig. 4. Diffuse reflectance spectrum of P-TiO_2, P-$TiO_{2-x}N_x$, F-TiO_2 and F-$TiO_{2-x}N_x$ (a) and F-TiO_2 and F-$TiO_{2-x}N_x$ first derivative (b) as a function of wavelength λ. E_{gI}, E_{gIII}, E_{gII} refers to anatase, rutile and N-doping band gap.

on the catalyst's surface [19]. The position and the intensity of the O 1s peaks remained unchanged after ammonolysis. The N 1s was positioned at 395.9 eV as can be seen in the Fig. 3. The mechanism of nitrogen incorporation into the TiO_2 lattice (substitutional or interstitial) is still under discussion [5] as well as the effect of N-incorporation on the electronic structure of the TiO_2 [6]. Nevertheless, the position of the N 1s at about 397.7 eV has been associated by Asahi et al. [1] with a substitutional β-N state and related to the photocatalytic activity in the visible range. The composition of F-$TiO_{2-x}N_x$ in the present study was determined as $TiO_{1.995}N_{0.005}$.

It was already mentioned, that a change in colour of the ammonolysed powders was observed and confirmed by diffuse reflection spectroscopy (DRS). One can see in Fig. 4, that F-TiO_2 shows higher light absorption than P-TiO_2, but the fundamental absorption related to the band gap is the same. In the case of the N-doped powder, two effects can be distinguished. At first, the extinction of the fundamental absorption to higher wavelengths due to increased density of the states in the forbidden band gap, characterized by an absorption tail. Secondly, the formation of a distinctive absorption band can be seen. The measured diffusive reflectance according to Radecka et al. [20] can be used directly for the band gap estimation. The maximum value of the plot of the differential reflectance $dR/d\lambda$ as a function of λ corresponds to the band gap of the semiconductor material (Fig. 4). This method of band gap evaluation has been applied mainly to well crystalline semiconductor materials.

The band gap energy can also be evaluated by another method, the so-called Tauc plot, i.e., a plot of $(\alpha h\nu)^{1/\gamma}$ as a function of photon energy $h\nu$ [21,22]. This method assumes that the absorption product $\alpha h\nu$ is given by:

$$\alpha h\nu = \alpha_0 (h\nu - E_g)^{\gamma} \quad (1)$$

where α_0 is a material constant (10^5 to 10^6 cm^{-1} eV^{-1} for typical oxide semiconductors), the power coefficient γ can be: 1/2, 3/2, 2 or 3 depending on the type of transition: direct allowed, direct forbidden, indirect allowed or indirect forbidden, respectively. Eq. (1) is only valid over the strong absorption region and was originally used for the amorphous semiconductors [21,22]. The Kubelka–Munk function was applied for thick samples to convert diffusive reflectance measurements into the equivalent absorption coefficient [23,24]:

$$\alpha \sim \frac{K(\lambda)}{S(\lambda)} = \frac{(1 - R_\infty)^2}{2R_\infty} \quad (2)$$

where K and S are the absorption and scattering coefficients for the measured sample and the reflectance $R_\infty = R/R_{ref}$. If the weak dependence of the scattering coefficient S on the wavelength is taken into account, K/S can be assumed then as proportional to the absorption within the narrow range, which is containing the fundamental absorption edge.

Based on the first described method two band gaps were calculated for the F-TiO_2, which consists of 91 wt.% of anatase and 9 wt.% of rutile and related to the two possible electron transitions at 3.28 and 3.17 eV, these values can be assigned to anatase and rutile phase, respectively (Fig. 4). The same phenomena can be observed for the P-TiO_2 powder (Table 2). For F-$TiO_{2-x}N_x$ and P-$TiO_{2-x}N_x$ nanopowders, the differential reflectance showed two maxima, what is interpreted as a two-phase material or two different types of the electron transition [25]. The calculated E_g values are comparable to E_g of TiO_2 and of $TiO_{2-x}N_x$ as reported in literature [1,6,20,26]. According to some theories [27,28] the observed blue shift of the fundamental absorption edge of TiO_2 can be related to the decrease in the average crystallite size, i.e., some of the particles are in the range of the 5–10 nm which can cause a shift of the E_g of about 0.2 eV to higher energies, due to so-called

Table 2
Summary of band gap E_g and power coefficient γ calculation for pure and N-doped TiO_2 nanopowders (Fig. 4).

Sample	E_g (eV)					γ
		$(\alpha h\nu)^{1/2}$, $\gamma = 2$	$(\alpha h\nu)^{2/3}$, $\gamma = 3/2$	$(\alpha h\nu)^2$, $\gamma = 1/2$	$dR/d\lambda$	
F-TiO_2	E_{gI}	3.04 ± 0.04	3.13 ± 0.09	3.41 ± 0.10	3.17 ± 0.01	0.582 ± 0.025
	E_{gII}	–	–	–	–	–
	E_{gIII}	–	–	–	3.28 ± 0.01	0.895 ± 0.026
F-$TiO_{2-x}N_x$	E_{gI}	2.73 ± 0.05	2.96 ± 0.04	3.37 ± 0.10	3.43 ± 0.01	0.923 ± 0.008
	E_{gII}	1.93 ± 0.01	2.12 ± 0.01	2.56 ± 0.10	2.43 ± 0.01	1.490 ± 0.005
	E_{gIII}	–	–	–	–	–
P-TiO_2	E_{gI}	3.03 ± 0.05	3.13 ± 0.14	3.47 ± 0.10	3.14 ± 0.01	0.927 ± 0.030
	E_{gII}	–	–	–	–	–
	E_{gIII}	–	–	–	3.35 ± 0.01	0.846 ± 0.003
P-$TiO_{2-x}N_x$	E_{gI}	2.85 ± 0.06	3.06 ± 0.07	3.45 ± 0.10	3.39 ± 0.01	0.657 ± 0.008
	E_{gII}	1.83 ± 0.01	2.06 ± 0.01	2.63 ± 0.09	2.55 ± 0.01	0.506 ± 0.007
		–	2.79 ± 0.01	–	–	1.494 ± 0.044
	E_{gIII}	–	–	–	–	–

quantum size effect. However, Serpone et al. [29] argued that there are no size quantization effects on the spectral properties of TiO_2. They ascribed the blue shift in the colloidal TiO_2 to a direct interband transition in an otherwise indirect band gap semiconductor.

Before applying the Tauc plot for the forbidden band gap calculation one should note that semiconductors are classified as materials only with direct ($\gamma = 0.5$) or indirect ($\gamma = 2$) allowed transition [29]. For nanoscale semiconductors most authors assume indirect transition for the calculation of the band gap and the Tauc plot is subsequently applied as $(\alpha h\nu)^{1/2}$ vs. $h\nu$. E_g is estimated then from the intercept with the x-axis ($\alpha = 0$) of the straight line fitted from the linear region [30–33]. But is the assumption of an indirect transition correct? As mentioned already, Serpone et al. [29] answered that this is not necessarily the case. They have shown that for indirect band gap semiconductors like anatase, a direct transition can appear, when it is in a colloidal nanomaterial form. To clarify this question from above for the nanoparticles, the calculation of γ has been performed (Table 2) by inserting E_g into Eq. (1), as it was obtained from differential reflectance. On base of these calculations, one can see that there is no simple interpretation of γ and resulting electronic transitions in the investigated materials. According to data listed in Table 2, γ can be classified into three types: $\gamma \sim 0.5$; $\gamma \sim 1$ and $\gamma \sim 1.5$. Both $\gamma \sim 0.5$ and $\gamma \sim 1.5$ are corresponding to direct allowed and direct forbidden transition, respectively. Whereas $\gamma \sim 1$ has not simple interpretation. This value may result of mixed type of transition, e.g., degenerated direct forbidden transition or a kind of transition between direct and indirect allowed, which is not possible to be distinguished by performed calculations. Further studies are needed to explain this issue. Similar results were observed by Tang et al. [34]. They discussed the optical properties in rutile and anatase. Rutile has a band gap with transition close to indirect allowed. Due to the weak strength of the direct forbidden transition, the indirect transition dominates in the optical absorption just above the absorption edge. Also, Zak-rzewska [26] claimed that indirect allowed and direct forbidden transitions are possible in the anatase form.

Moreover, the different phase composition as well as the different crystallite size of anatase and rutile phase for F-TiO_2 and P-TiO_2 may have an impact on obtained numerical results. A significant change in the transition for the N-doped powders was observed for E_{gII}. For the F-$TiO_{2-x}N_x$ and P-$TiO_{2-x}N_x$ nanopowders the direct forbidden transition was observed. However, in case of P-$TiO_{2-x}N_x$ the additional direct allowed transition ($\gamma = 0.506$) can be distinguished.

Inserting theoretical values of γ: 1/2, 3/2 and 2 into Eq. (1) the E_g values were estimated (Table 2). Effect of assumed γ value on obtained E_g is pronounced.

The photocatalytic activity of pure and N-doped TiO_2 nanopowders was evaluated by measuring decolourisation rate of methylene blue (MB) as an aqueous solution. The negative time (−10 min) indicates the time where adsorption of the dye takes place, while the reactor was not irradiated (Fig. 5). It should be noted that the dye adsorption on the F-TiO_2 and F-$TiO_{2-x}N_x$ surface is much higher than on the P-TiO_2 and P-$TiO_{2-x}N_x$ surface. The specific surface area (SSA) of both powders before ammonolysis is at a comparable level of about 50 $m^2\ g^{-1}$. The higher adsorption can be related to a higher affinity of the dye to the surface, which is affiliated with a higher number of active centres on the photocatalyst's surface. According to Yan et al. as well as Mills and Wang [35,36] photocatalytic decomposition of MB occurring within 400–500 nm is only negligibly affected by photosensitising effect. Therefore, the photodecolourisation of the MB can be mainly assigned to the photoactivity of the used photocatalysts. Fig. 5 shows that the photoactivity of F-TiO_2 is much higher than of

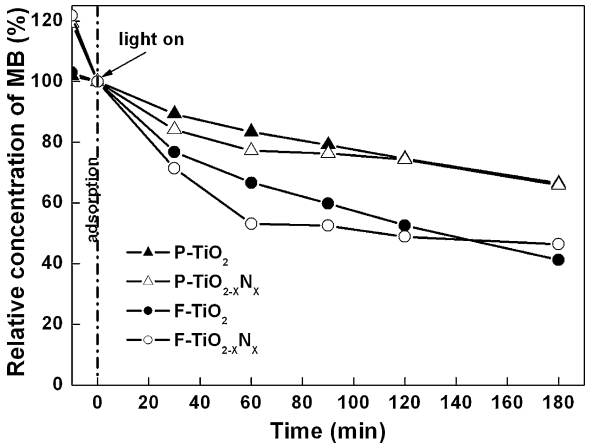

Fig. 5. Photodecolourisation of methylene blue under visible light by pure and N-doped photocatalysts.

P-TiO_2 photocatalyst. The differences between the photocatalysts can be associated with the phase composition, particle morphology and the average crystallite size. The enhanced photoactivity of F-TiO_2 can be related to the better absorption of the light in the visible range in comparison to P-TiO_2 (Fig. 4), which may origin from the number of defects occurring in the nanoscale material. The higher amount of anatase in F-TiO_2 can also be the reason of the improvement of the photoactivity thanks to convenient position of the conduction band regarding the reduction potential of water. For the ammonolysed powder, an increase in the photodecolourisation of MB in the first 60 min can be observed, compared to the undoped one. The increase of the photoactivity of P-$TiO_{2-x}N_x$ is not significant in contrast to F-$TiO_{2-x}N_x$. Nevertheless, after 60 min of the reaction both N-doped photocatalysts seemed to be deactivated. The enhanced photocatalytic activity in the range of 400–500 nm for the N-doped TiO_2 nanopowders can be related to the improved light absorption in this range (Fig. 4 and Table 2). Nevertheless, substitutional introduction of N into the TiO_2 structure proved by XPS measurements – N 1s at 395.9 eV (Fig. 3) followed by increase number of defects, which on the one hand can improve the light absorption in the visible range due to the modification of the electronic structure of TiO_2. And on the other too high concentration of defects can drive the faster recombination of the charge carriers. The low enhancement of the photoactivity in the vis region in the presence of water was already reported [4,37]. Where Tachikawa et al. [38] observed that the photoassited oxidation of organic compounds on the $TiO_{2-x}N_x$ surface proceed from oxygen reduction acting as an electron scavenger and creating the $O_2^{\bullet -}$ radical which through the reaction with water produce the $OH^{\bullet -}$ radical. The water photoreduction through the reaction with holes did not occurred due to the trapping of the h^+ by the N-introduced levels in the band gap. Moreover the hole generated by the visible light irradiation is less mobile than the one generated by UV irradiation [39].

4. Conclusions

N-doped TiO_2 of the composition $TiO_{1.995}N_{0.005}$ photocatalysts have been produced by successful ammonolysis of titania nanoparticles. According to XPS analysis the position at 395.9 eV of N 1s can be related to the substitutional nitrogen incorporation. Both $TiO_{2-x}N_x$ nanopowders show a shift of the light absorption towards visible region. Based on carried out calculations, the authors assume that a very careful judgment is required about the electron transition type in the semiconductor materials, as well as on the E_g estimation, which is related to it. It is established that

F-TiO_2 has two allowed gaps with direct forbidden or indirect allowed transition. The electronic structure revealed that P-TiO_2 showed a direct allowed transition with direct forbidden or indirect allowed transition. On the other hand, it arose that nitrogen-doped materials allow two new transitions: direct allowed and direct forbidden. The differential reflectance method seems to be the best for the band gap estimation. Based on differential reflectance data, the additional band gap at 2.43 eV for F-$TiO_{2-x}N_x$ and 2.55 eV for P-$TiO_{2-x}N_x$ has been estimated, which can be related to occurrence of new electron transition due to N-doping. Photocatalytic activity of ammonolysed powders was slightly higher comparable to starting materials, where the flame spray synthesised (FSS) powders, the F-TiO_2 and F-$TiO_{2-x}N_x$ performed much better that P-TiO_2 and P-$TiO_{2-x}N_x$. The low enhancement of the photoactivity of the N-doped TiO_2 nanopowders in the 400–500 nm region resulted from lack of the water photooxidation through the reaction with holes which is limited by the trapping of the h^+ by the N-introduced levels in the band gap.

Acknowledgement

The authors want to acknowledge Davide Ferri and Safer Mourad for the scientific discussions, the International PhD School Switzerland-Poland and the Polish Ministry of Science and Higher Education (N N508 1845 33) for the financial support.

References

[1] R. Asahi, T. Morikawa, t. Ohwaki, K. Aoki, Y. Taga, Science 293 (2001) 269.
[2] M. Batzill, E.H. Morales, U. Diebold, Phys. Rev. Lett. 96 (2006) 026103.
[3] B. Kosowska, S. Mozia, A.W. Morawski, B. Grzmil, M. Janus, K. Kalucki, Sol. Energy Mater. Sol. Cells 88 (2005) 269.
[4] M. Mrowetz, W. Balcerski, A.J. Colussi, M.R. Hoffmann, J. Phys. Chem. B 108 (2004) 17269.
[5] F. Peng, L. Cai, H. Yu, H. Wang, J. Yang, J. Solid State Chem. 181 (2008) 130.
[6] N. Serpone, J. Phys. Chem. B 110 (2006) 24287.
[7] K.K. Akurati, A. Vital, J.-P. Dellemann, K. Michalow, T. Graule, D. Ferri, A. Baiker, Appl. Catal. B 79 (2008) 53.
[8] K.A. Michalow, A. Vital, A. Heel, T. Graule, F.A. Reifler, A. Ritter, K. Zakrzewska, M. Rekas, J. Adv. Oxid. Technol. 11 (2008) 56.
[9] D. Logvinovich, A. Borger, M. Dobeli, S.G. Ebbinghaus, A. Reller, A. Weidenkaff, Prog. Solid State Chem. 35 (2007) 281.
[10] P. Thompson, D.E. Cox, J.B. Hastings, J. Appl. Crystallogr. 20 (1987) 79.
[11] B.V. Laar, W.B. Yelon, J. Appl. Crystallogr. 17 (1984) 47.
[12] L.W. Finger, D.E. Cox, A.P. Jephcoat, J. Appl. Crystallogr. 27 (1994) 892.
[13] J. Rodriguez-Carvajal, T. Roisnel, Mater. Sci. Forum 442–444 (2004) 123.
[14] J. Rodriguez-Carvajal, Physica B (1993) 55.
[15] A. Mills, S. Morris, R. Davies, J. Photochem. Photobiol. A 70 (1993) 183.
[16] J.L. Gole, J.D. Stout, C. Burda, Y. Lou, X. Chen, J. Phys. Chem. B 108 (2004) 1230.
[17] E. Finazzi, C. DiValentin, A. Selloni, G. Pacchioni, J. Phys. Chem. C 111 (2007) 9275.
[18] V.I. Bukhtiyarov, Catal. Today 56 (2000) 403.
[19] J. Yu, H. Yu, B. Cheng, M. Zhou, X. Zhao, J. Mol. Catal. A: Chem. 253 (2006) 112.
[20] M. Radecka, M. Rekas, K. Zakrzewska, Trends Inorg. Chem. 9 (2006) 81.
[21] J. Tauc, Mater. Res. Bull. 5 (1970) 721.
[22] J. Tauc, R. Grigorovici, A. Vancu, Phys. Stat. Sol. 15 (1966) 627.
[23] A.B. Murphy, Appl. Opt. 46 (2007) 3133.
[24] P. Kubelka, J. Opt. Soc. Am. 28 (1948) 448.
[25] S. Komornicki, M. Radecka, P. Sobas, Mater. Res. Bull. 39 (2004) 2007.
[26] K. Zakrzewska, Titanium Dioxide Thin Films for Gas Sensors and Photonic Application, AGH-Univeristy of Science and Technology, Cracow, 2003, p. 191.
[27] K. Reddy Madhusudan, C.V. Reddy Gopal, S.V. Manorama, J. Solid State Chem. 158 (2001) 180.
[28] M. Radecka, K. Zakrzewska, M. Wierzbicka, A. Gorzkowska, S. Komornicki, Solid State Ionics 157 (2003) 379.
[29] N. Serpone, D. Lewless, R. Khairutdinov, J. Phys. Chem. 99 (1995) 16646.
[30] R. Bacsa, J. Kiwi, T. Ohno, P. Albers, V. Nadtochenko, J. Phys. Chem. B 109 (2005) 5994.
[31] W.Y. Teoh, R. Amal, L. Madler, S.E. Pratsinis, Catal. Today 120 (2007) 203.
[32] C.-C. Pan, J.C.S. Wu, Mater. Chem. Phys. 100 (2006) 102.
[33] S. Sakthivel, M. Janczarek, H. Kisch, J. Phys. Chem. B 108 (2004) 19384.
[34] H. Tang, K. Prasad, R. Sanjines, P.E. Schmid, F. Levy, J. Appl. Phys. 75 (1994) 2042.
[35] X. Yan, T. Ohno, K. Nishijima, R. Abe, B. Ohtani, Chem. Phys. Lett. 429 (2006) 606.
[36] A. Mills, J. Wang, J. Photochem. Photobiol. A 127 (1999) 123.
[37] A.V. Emeline, V.N. Rybchuk, N. Serpone, Int. J. Photoenergy, doi:10.1155/2008/258394.
[38] T. Tachikawa, M. Fujitsuka, T. Majima, J. Phys. Chem. C 111 (2007) 5259.
[39] C.D. Valentin, E. Finazzi, G. Pacchioni, A. Selloni, S. Livraghi, M.C. Paganini, E. Giamello, Chem. Phys. 339 (2007) 44.